P H Y S I C A L   R E V I E W   L E T T E R S

Shape Memory and Pseudoelasticity in Metal Nanowires

Harold S. Park,[1,*] Ken Gall,[2] and Jonathan A. Zimmerman[3]

[1]*Department of Civil and Environmental Engineering, Vanderbilt University, Nashville, Tennessee 37235, USA*
[2]*School of Materials Science and Engineering, Woodruff School of Mechanical Engineering, Georgia Institute of Technology,*
Atlanta, Georgia 30332, USA
[3]*Sandia National Laboratories, Livermore, California 94551, USA*

Structural reorientations in metallic fcc nanowires are controlled by a combination of size, thermal energy, and the type of defects formed during inelastic deformation. By utilizing atomistic simulations, we show that certain fcc nanowires can exhibit both shape memory and pseudoelastic behavior. We also show that the formation of defect-free twins, a process related to the material stacking fault energy, nanometer size scale, and surface stresses is the mechanism that controls the ability of fcc nanowires of different materials to show a reversible transition between two crystal orientations during loading and thus shape memory and pseudoelasticity.

Various researchers have demonstrated that fcc nanowires can undergo unique structural reorientations and transformations based on size and thermal energy [1–6]. For example, $\langle 100 \rangle$ gold nanowires were found to transform into a body-centered tetragonal (BCT) structure [4,6] if the cross sectional dimensions of the wire are smaller than about 2.0 nm. At a critical temperature that is a function of the wire cross sectional length, $\langle 100 \rangle$ copper nanowires were found to reorient into $\langle 110 \rangle$ wires with $\{111\}$ surfaces [5]; the reoriented $\langle 110 \rangle / \{111\}$ wires were found to exhibit pseudoelasticity upon application and subsequent removal of tensile loading. Here, we use atomistic simulations of gold, copper, and nickel to reveal the propensity of various metallic fcc nanowires to experience recovery of large inelastic deformation during unloading (pseudoelasticity) or after subsequent heating (shape memory). These materials were chosen due to their disparate stacking fault energies (SFEs) (gold = 32 mJ/m², copper = 45 mJ/m², nickel = 125 mJ/m² [7]), where the SFE is the energetic barrier to partial dislocation nucleation and propagation. In polycrystalline materials, twinning is often seen in low SFE materials [8]; in single crystal nanowires, we show here that low SFE gold nanowires form multiple partial dislocation systems during the $\langle 100 \rangle$ to $\langle 110 \rangle / \{111\}$ reorientation, thus mitigating the reversibility between $\langle 100 \rangle$ and $\langle 110 \rangle / \{111\}$ configurations by creating twins with interior $\{111\}$ stacking faults that make the reversible transformation paths necessary for shape memory and pseudoelasticity more difficult. On the other hand, it is shown that copper and nickel, which have higher SFEs, form twins without interior defects which facilitates a high degree of reversibility owing to the ability to freely move twin boundaries without formation of irreversible defect structures.

As indicated in Fig. 1, and will be demonstrated in this work, pseudoelasticity and shape memory in fcc nanowires can be made possible by a reversible reorientation between a higher energy $\langle 100 \rangle$ orientation and a lower energy

$\langle 110 \rangle / \{111\}$ orientation. At a critical temperature T_c, thermal energy combined with intrinsic surface stresses can spontaneously reorient a wire with an initial $\langle 100 \rangle$ axis into a wire with a $\langle 110 \rangle$ axis and $\{111\}$ surfaces. The driving force for the reorientation is a reduction in surface energy realized by the exposure of lower energy $\{111\}$ surfaces in the new $\langle 110 \rangle$ wire. Starting from a $\langle 110 \rangle / \{111\}$ wire, applied deformation results in reverse reorientation of the wire from $\langle 110 \rangle / \{111\}$ back to $\langle 100 \rangle$ (Step 1). If the temperature during reverse reorientation is in the vicinity of T_c, the new $\langle 100 \rangle$ wire is unstable under its own surface stresses, and unloading will result in spontaneous reorientation back to $\langle 110 \rangle / \{111\}$, a pseudoelastic response (Step 2). If the deformation temperature is sufficiently below T_c, the new $\langle 100 \rangle$ wire is stable under its own surface stresses, and will remain a $\langle 100 \rangle$ wire after unloading (Step 2). As the wire is heated, the $\langle 100 \rangle$ wire will reorient to $\langle 110 \rangle / \{111\}$ at T_c, a shape memory response (Step 3). The processes illustrated in Fig. 1 will only occur if the nanowire has a small enough cross sectional area so surface stresses cause instability of the $\langle 100 \rangle$ orientation at a
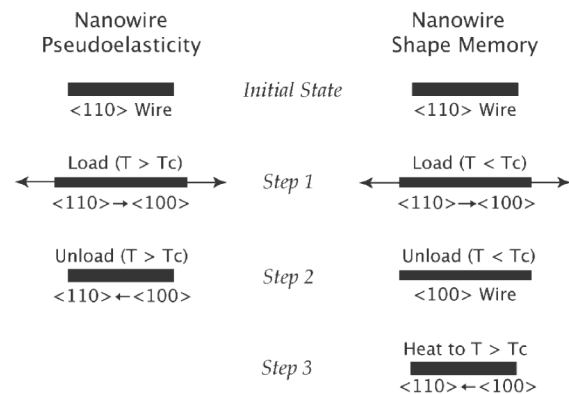

FIG. 1.   Schematic of shape memory and pseudoelasticity in fcc metal nanowires.

TABLE I. Intrinsic (γ_{sf}) and unstable (γ_{usf}) stacking fault energies and ratios (γ_{usf}/γ_{sf}), {100} (γ_{100}) and {111} (γ_{111}) surface energies and ratios ($\gamma_{111}/\gamma_{100}$) for EAM potentials of nickel, copper, and gold. T_c/T_m calculated for $6 \times 6 \times 50$ cubic lattice unit nanowires. Energetic units are in mJ/m^2 and the experimentally measured melt temperature T_m has units of K.

Metal	γ_{sf}	γ_{usf}	γ_{100}	γ_{111}	T_c/T_m	T_m	$\gamma_{111}/\gamma_{100}$	γ_{usf}/γ_{sf}
Gold	32	92	1090	1180	0.0374	1337	0.924	2.88
Copper	39	133	1351	1452	0.3134	1356	0.930	3.43
Nickel	125	264	1928	2060	0.4345	1726	0.936	2.11

temperature below the melting temperature of the nanowire. Specifically, the pseudoelasticity and shape memory effects disappear at a rate directly proportional to the inverse of wire diameter since the surface stress-induced driving force for the transition between the two wire states also diminishes at a rate directly proportional to the inverse of wire diameter [6].

We investigate the fundamental mechanisms controlling shape memory and pseudoelasticity in fcc metal nanowires via molecular dynamics (MD) simulations using embedded atom (EAM) [9] potentials for gold [10], nickel [11], and copper [12]; relevant potential parameters are summarized in Table I. The potentials were chosen for their accurate representations of the materials respective SFEs. The wires were created using atomic positions from a bulk fcc crystal with an initial $\langle 100 \rangle$ orientation, square cross section, and {100} surfaces. The wire length was 50 cubic lattice units long in the z direction, with cross sectional lengths less than or equal to 6 cubic lattice units in the x and y directions; no periodic boundary conditions were utilized at any stage in the simulations, which were performed using the Sandia-developed code WARP [13,14]. We note that the numerically determined values for T_c in Table I represent lower bound estimates for each material; this is because EAM potentials typically underestimate surface stresses [15] while also lacking fidelity in thermal transport properties.

We first demonstrate that $\langle 100 \rangle$ wires can reorient to the energetically favorable $\langle 110 \rangle/\{111\}$ orientation at T_c. By constraining the wire ends to move only in the z direction and applying a velocity scaling thermostat at T_c, the $\langle 100 \rangle$ nanowires contract in the z direction, eventually reorienting to $\langle 110 \rangle/\{111\}$ nanowires; an example of the reorientation process via twinning is shown in Figs. 2(a)–2(d) for a 1.76 nm $\times$ 1.76 nm nickel nanowire at 640 K. The boundary conditions were chosen to mimic the situation of a nanowire bonded to connected leads that permit extension or contraction of the wire while constraining the wire ends to move in axial directions only. The thermoelectromechanical nature of this connection will play an important role in influencing the shape memory behavior of the nanowires, and should be investigated in future experimental and theoretical studies.

The reorientation begins with the formation of a single twin in the wire interior which gradually increases in size to allow the complete $\langle 100 \rangle$ to $\langle 110 \rangle\{111\}$ reorientation to occur. Gold and copper also reoriented from $\langle 100 \rangle$ to

$\langle 110 \rangle\{111\}$ via the formation of twins at temperatures close to their respective T_c. The difference in T_c for copper and gold, which have similar SFEs, is due to the fact that the {100} surface stress for gold is nearly double that of copper [15], indicating that less thermal energy is needed to assist the surface stresses in forming the lower energy {111} surfaces. Below T_c, the wires partially reorient via spatially distributed twinning from $\langle 100 \rangle$ to $\langle 110 \rangle/\{111\}$, where twin boundaries in the nanowire separate $\langle 100 \rangle$ and $\langle 110 \rangle/\{111\}$ single crystals.

After reorientation was completed, the $\langle 110 \rangle/\{111\}$ nanowires were loaded in tension in the z direction to test for pseudoelastic behavior. Pseudoelasticity is demonstrated if the $\langle 110 \rangle/\{111\}$ wires can reorient back to the initial, defect-free $\langle 100 \rangle$ orientation under external stress at a temperature greater than T_c as it was already demonstrated that wires will return to the $\langle 110 \rangle/\{111\}$ orientation once the external loading is removed at this temperature. Figures 3(g)–3(i) show that the 2.45 nm $\times$ 2.45 nm gold nanowire eventually fails via the formation and subsequent fracture of thin atom thick chains [10] before complete reorientation back to $\langle 100 \rangle$ can occur. Interestingly, only a minimal amount of detwinning is observed during the reorientation back to $\langle 100 \rangle$ is seen in Fig. 3(i), even though the initial reorientation from $\langle 100 \rangle$ to $\langle 110 \rangle/\{111\}$ was twinning dominated.

In contrast, nickel and copper both show different behavior during tensile loading of the reoriented $\langle 110 \rangle/\{111\}$ nanowire; the stress-induced reorientation from
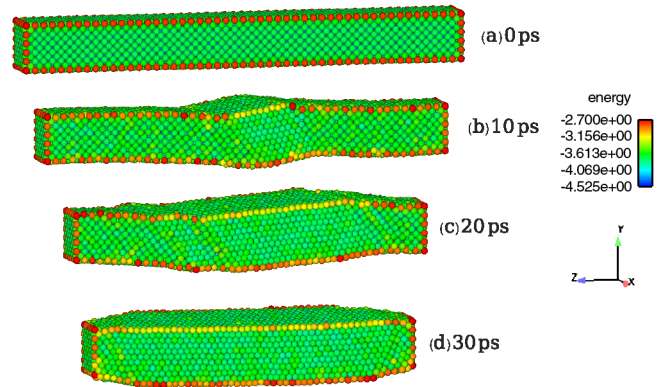

FIG. 2 (color online). Steps (a)–(d) show snapshots of the $\langle 100 \rangle$ to $\langle 110 \rangle/\{111\}$ thermal reorientation process at 640 K for 1.76 nm $\times$ 1.76 nm nickel nanowire. The potential energy values are in eV.
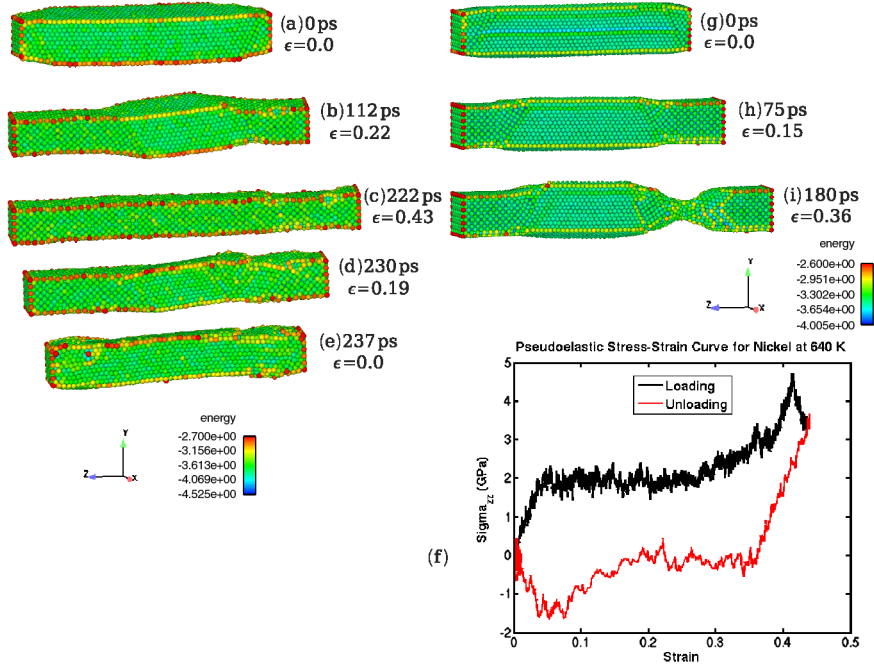
FIG. 3 (color online). Illustration of pseudoelastic behavior in nickel, while pseudoelasticity is not observed in gold. Steps (a)–(c) show successful stress-induced $\langle 110 \rangle / \{111\}$ to $\langle 100 \rangle$ reorientation in 1.76 nm × 1.76 nm nickel nanowires at 640 K. Steps (c)–(e) show reverse reorientation from $\langle 100 \rangle$ to $\langle 110 \rangle / \{111\}$ in nickel upon removal of the applied load; the entire loading/unloading process for nickel is shown in the stress-strain curve in snapshot (f). Steps (g)–(i) show the unsuccessful stress-induced $\langle 110 \rangle / \{111\}$ to $\langle 100 \rangle$ reorientation in 2.45 nm × 2.45 nm gold nanowires at 50 K. Potential energy values are in eV.

$\langle 110 \rangle / \{111\}$ back to the original $\langle 100 \rangle$ configuration is illustrated for a 1.76 nm × 1.76 nm nickel nanowire at 640 K at a strain rate of $\dot{\epsilon} = 10^9$ s^{-1} in Figs. 3(a)–3(c). As seen in Fig. 3(b), nickel is able to obtain its original $\langle 100 \rangle$ configuration by the creation and subsequent annihilation of twins as reported for copper by Liang and Zhou [5]. Upon continued tensile loading, the twin boundaries are pushed together, and finally annihilate each other to allow complete reorientation back to the original $\langle 100 \rangle$ configuration. After the original $\langle 100 \rangle$ orientation is reached, the load is removed. Because the nickel wire is above the critical reorientation temperature T_c, it reorients back to the $\langle 110 \rangle / \{111\}$ configuration in Figs. 3(c)–3(e) following the unloading stress-strain path seen in Fig. 3(f). The pseudoelastic loop seen in Fig. 3(f) is the same observed when bulk shape memory alloys are deformed above their austenite finish temperature and experience a forward and reverse thermoelastic martensitic transformation. The reverse loading from $\langle 110 \rangle / \{111\}$ to $\langle 100 \rangle$ was tested over three decades of strain rates from 10^8 s^{-1} to 10^{10} s^{-1}; the strain rates did not appear to deleteriously affect the shape memory or pseudoelastic behavior.

In order to test for shape memory effects, the reoriented $\langle 110 \rangle / \{111\}$ wires were thermally equilibrated at 10 K ($T < T_c$, Fig. 1) for 60 ps before tensile loading. The wires were loaded in tension at a strain rate of 10^9 s^{-1} as shown in Figs. 4(a)–4(c) for copper, and reached the initial $\langle 100 \rangle$ orientation at which point loading was removed. The resulting stress-induced 1.81 nm × 1.81 nm $\langle 100 \rangle$ wire in Fig. 4(c) is stable at very low temperatures with respect to T_c. Finally, the temperature of the stable $\langle 100 \rangle$ wire was increased by 50 K every 100 ps until complete reorientation back to $\langle 110 \rangle / \{111\}$ occurred as shown in Figs. 4(d)–4(f); the reorientation occurs via the initiation and propa-

gation of twins as in Fig. 2. The wire shows shape memory since it is capable of being deformed to nearly 40% strain through a reorientation to $\langle 100 \rangle$ while subsequent heating causes reverse reorientation back to $\langle 110 \rangle / \{111\}$.

To answer why nickel and copper exhibit shape memory and pseudoelasticity while gold does not despite the fact that all three materials reoriented from $\langle 100 \rangle$ to $\langle 110 \rangle / \{111\}$ via twinning, we analyzed the initial defect structure formed in each material during the original $\langle 100 \rangle$ to $\langle 110 \rangle \{111\}$ reorientation. We find that the initial defect structure formed during the $\langle 100 \rangle$ to $\langle 110 \rangle / \{111\}$ reorien-
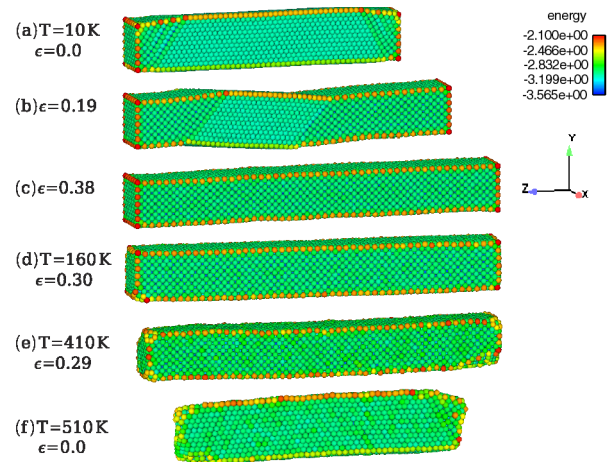

FIG. 4 (color online). Illustration of the shape memory behavior seen in initially 1.81 nm × 1.81 nm $\langle 100 \rangle$ copper nanowires. Steps (a)–(c) correspond to loading the reoriented $\langle 110 \rangle / \{111\}$ nanowire at 10 K in tension. Steps (c)–(f) correspond to heating the resulting $\langle 100 \rangle$ nanowire until reoriented $\langle 110 \rangle / \{111\}$ nanowire is obtained, demonstrating the shape memory effect. Potential energy values are in eV.
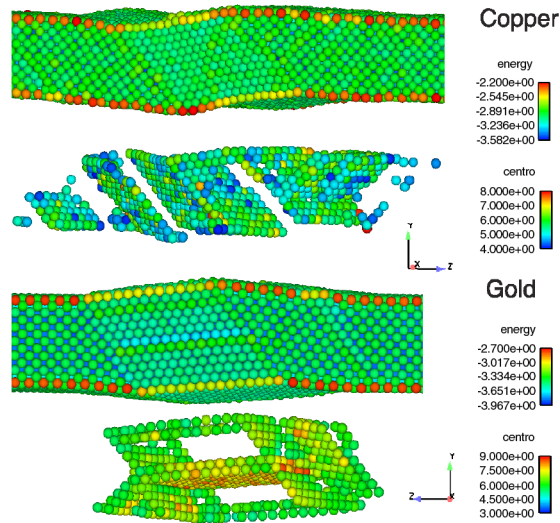
FIG. 5 (color online). Snapshot of the ⟨100⟩ to ⟨110⟩/{111} reorientation for gold and copper. Potential energy values are in eV; the centrosymmetry parameter is defined in [16].

tation controls the shape memory and pseudoelastic behavior of the material. A snapshot of the initial defect structure at $t = 25$ ps during the ⟨100⟩ to ⟨110⟩/{111} reorientation is shown for the 2.45×2.45 nm gold and 1.81 nm $\times$ 1.81 nm copper nanowires in Fig. 5. While the copper wire has formed multiple twins, each twin has a defect-free interior as visualized using the centrosymmetry parameter [16], a measure of local atomic coordination where a value of zero indicates a fully coordinated atom.

In contrast, the gold twin shows a distinct {111} stacking fault within the twin interior. We verified that the interior {111} stacking fault resulted in the inability to regain the initial ⟨100⟩ orientation by gradually reloading the wires in tension after initial defect nucleation during the ⟨100⟩ to ⟨110⟩/{111} reorientation for all materials. Upon tensile reloading of the partially reoriented ⟨110⟩/{111} nanowires, it was found that copper and nickel still regained their initial defect-free ⟨100⟩ orientations, while gold, due to the more complex defect and stacking fault structure in the twin interior, did not regain the initial ⟨100⟩ orientation.

In summary, we have shown that metallic fcc nanowires can show shape memory and pseudoelastic behavior through the formation of defect-free twins during the ⟨100⟩ to ⟨110⟩/{111} reorientation process. Gold, which has a lower SFE than copper and nickel, was shown to form twins with interior {111} stacking faults, while the higher SFE copper and nickel nanowires formed defect-free twins; other factors such as ratios of SFE and twinning energies may also play critical roles in this process [17,18]. The defect-free twins can then be annihilated during the stress-driven ⟨110⟩/{111} to ⟨100⟩ reorientation, allowing the loading/unloading cycle required for shape memory and pseudoelastic behavior to continue. It is critical to note that the present results imply that standard metals at the nanoscale may exhibit both reversible shape memory

behavior previously observed only in exotic alloys such as NiTi [19] as well as pseudoelasticity and pseudoelastic strains previously observed only in polycrystalline shape memory alloys [19] and copper nanowires [5]; these effects are not observed by the metals in bulk form. In addition, the theoretical maximum recoverable strain in NiTi is approximately 10%, while these nanowires have predicted recoverable strains on the order of 40%. Since researchers have more experience growing monolithic metallic nanowires, the potential of such wires to experience shape memory and pseudoelasticity is critical to guiding basic research efforts in nanoscience and nanotechnology.

---

*Electronic address: harold.park@vanderbilt.edu

[1] Y. Kondo and K. Takayanagi, Phys. Rev. Lett. **79**, 3455 (1997).

[2] Y. Kondo, Q. Ru, and K. Takayanagi, Phys. Rev. Lett. **82**, 751 (1999).

[3] A. Hasmy and E. Medina, Phys. Rev. Lett. **88**, 096103 (2002).

[4] J. Diao, K. Gall, and M. L. Dunn, Nat. Mater. **2**, 656 (2003).

[5] W. Liang and M. Zhou, J. Eng. Mater. Technol. **127**, 423 (2005).

[6] J. Diao, K. Gall, and M. L. Dunn, Phys. Rev. B **70**, 075413 (2004).

[7] J. P. Hirthe and J. Lothe, *Theory of Dislocations* (Krieger Publishing Company, Malabar, 1982), 2nd ed.

[8] J. W. Christian and S. Mahajan, Prog. Mater. Sci. **39**, 1 (1995).

[9] M. S. Daw and M. I. Baskes, Phys. Rev. B **29**, 6443 (1984).

[10] H. S. Park and J. A. Zimmerman, Phys. Rev. B **72**, 054106 (2005).

[11] J. E. Angelo, N. R. Moody, and M. I. Baskes, Model. Simul. Mater. Sci. Eng. **3**, 289 (1995).

[12] S. M. Foiles (to be published).

[13] S. J. Plimpton, J. Comput. Phys. **117**, 1 (1995).

[14] WARP computer code, http://www.cs.sandia.gov/~sjplimp/lammps.html, 2005.

[15] J. Wan, Y. L. Fan, D. W. Gong, S. G. Shen, and X. Q. Fan, Model. Simul. Mater. Sci. Eng. **7**, 189 (1999).

[16] C. L. Kelchner, S. J. Plimpton, and J. C. Hamilton, Phys. Rev. B **58**, 11 085 (1998).

[17] E. B. Tadmor and N. Bernstein, J. Mech. Phys. Solids **52**, 2507 (2004).

[18] H. V. Swygenhoven, P. M. Derlet, and A. G. Froseth, Nat. Mater. **3**, 399 (2004).

[19] K. Gall, H. Sehitoglu, Y. I. Chumlyakov, and I. Kireeva, Acta Mater. **47**, 1203 (1999).